Landslides (2022) 19:1897–1912
DOI 10.1007/s10346-022-01898-4
Received: 8 December 2021
Accepted: 1 May 2022
Published online: 17 May 2022

Xiaoyu Yi · Wenkai Feng · Mingtang Wu · Zhiping Ye · Yunfeng Fang · Ping Wang · Renjiang Li · Jiawei Dun

The initial impoundment of the Baihetan reservoir region (China) exacerbated the deformation of the Wangjiashan landslide: characteristics and mechanism

Abstract Reservoir landslides greatly threaten reservoir safety. Understanding the deformation characteristics and mechanism of reservoir landslides can help evaluate their stability and prevent secondary disasters. A detailed analysis of the deformation characteristics and landslide reactivation mechanism of the Wangjiashan (WJS) ancient landslide during the initial impoundment of the Baihetan Reservoir region was performed using comprehensive in situ monitoring and drilling data. The WJS landslide slowly deformed before impoundment. Reservoir impoundment was the main factor driving the intensifying deformation of the WJS landslide. The rise in reservoir water resulted in bank collapse at the landslide toe. After the reservoir water flooded the sliding zone of the landslide toe, creep deformation occurred along the deep sliding zone, which developed into overall sliding on July 7. The further rise in the reservoir water level has led to the rapid sliding of the landslide. The WJS landslide is a buoyancy weight-reducing landslide. When the reservoir water rises to a high level, the buoyancy force of the reservoir water acts on the resisting section, which reduces the resisting force and leads to the rapid sliding of the landslide. When the reservoir water level drops from the high level, the buoyancy acting on the resisting section decreases gradually, and the stability of the landslide can be restored. At present, the WJS landslide deformation rate gradually decreases with the reservoir water level, and the probability of large-scale landslides is low. However, WJS landslide monitoring needs to be strengthened to more closely study its deformation mechanism.

Keywords Baihetan Reservoir region · Wangjiashan landslide · Initial impoundment · Deformation characteristics · Deformation mechanism · Ancient landslide

Introduction

The experience gained from the construction and impoundment of many large hydropower stations shows that reservoir impoundment induces many nascent landslides and leads to the reactivation of many ancient landslides (Tang et al. 2019a). For example, in 1963, the Vaiont landslide in Italy underwent multiple accelerated deformations before final failure in the impoundment stage (Semenza and Ghirotti 2000). The Canelles reservoir landslide in Spain slipped during a rapid decrease in reservoir water to a low water level in 2006 (Pinyol et al. 2012). According to incomplete statistics, the high impoundment of the Three Gorges Reservoir in China has led to the reactivation of many ancient landslides after impoundment and has generated many new landslides, with more than 2000 water-related landslides in the reservoir area (Li et al. 2020). Among them, more than 200 landslides produced deformation in the Three Gorges Reservoir area during the first impoundment in 2003, and the Qianjiangping landslide also slid as a whole during this period, resulting in 14 deaths, ten missing persons, and more than 1200 people affected by tragedy (Wang et al. 2004, 2008; Yin et al. 2015).

The Baihetan Hydropower Station is located in Ningnan County, Sichuan Province, and Qiaojia County, Yunnan Province, China. It is the second hydropower station to be built in the lower reaches of the Jinsha River in China. The planned installed capacity of the Baihetan Hydropower Station is 16000 MW, making it the second-largest hydropower station in China after the Three Gorges Hydropower Station. Similar to those near the Xiluodu Hydropower Station and Wudongde Hydropower Station in the mainstream Jinsha River (Xie et al. 2016; Zhao et al. 2018; Yi et al. 2020), geohazards in the Baihetan Reservoir region are very prominent. Dun et al. (2021) used a time series of interferometric synthetic aperture radar (InSAR) data to detect active geological disasters in the Baihetan Reservoir region before impoundment and discovered many ancient landslides in the reservoir area. According to the construction plan, the minimum reservoir water level and maximum reservoir level are 765 m and 825 m, respectively. Some ancient landslides will reactivate under the effect of reservoir water level fluctuations.

On April 6, 2021, the Baihetan Reservoir began to impound water, and the reservoir water level started to rise from 660.35 m to its highest level of 816.51 m reached on September 30. During the first impoundment period of the reservoir, the deformation of the Wangjiashan (WJS) ancient landslide intensified. The monitored maximum horizontal deformation rate reached 857.90 mm/day, and its stability under impoundment was of wide concern to the authorities and residents in the Baihetan Reservoir region. Therefore, global navigation satellite system (GNSS) displacement monitoring, multitemporal unmanned aerial vehicle (UAV) photography, inclinometers, rain gauges, and groundwater level gauges were used to monitor the landslide activity in this area. Based on these multisource datasets, this paper analyzes the deformation process and characteristics of the WJS landslide and proposes a mechanism that could have led to the increased deformation of the WJS landslide by impoundment. The research described in this paper provides more insights into the study of impoundment stability and disaster prevention and the control of the WJS landslide.

Materials

Geological setting

The WJS landslide is located upstream of the Baihetan hydropower dam site in WJS village, Nagu town, Huize County, Yunnan Province, at a straight-line distance of approximately 80 km from the dam site (Fig. 1). Several faults have developed in this area; the right bank of the Jinsha River is mainly controlled by the Xiaojiang Fault (F5), and its secondary fault and the left bank of the Jinsha River are influenced by the Zemuhe Fault (F7). The Baihetan Reservoir region has a subtropical dry/warm river valley climate, with an average annual temperature ranging from 12 °C to 20 °C. The annual precipitation in the study area is approximately 600 ~ 800 mm; more frequent precipitation occurs from May to October, which can reach 90% of the annual rainfall, and clear and dry weather occurs from November to April, when rainfall is scarce.

General description of the landslide

The WJS landslide is located on the right bank slope of the Xiaojiang River, a tributary of the Jinsha River. As shown in Fig. 2, the WJS landslide is an ancient landslide with significant features. The back edge of the ancient landslide mound is 1125 m, and the upper part is a steep bedrock wall with a slope of approximately 40–50°. The front edge of the landslide is the Xiaojiang River and the G248 National Highway, with an elevation of 732 m. The steep part of the slope, with a slope of approximately 35–45°, is steeper

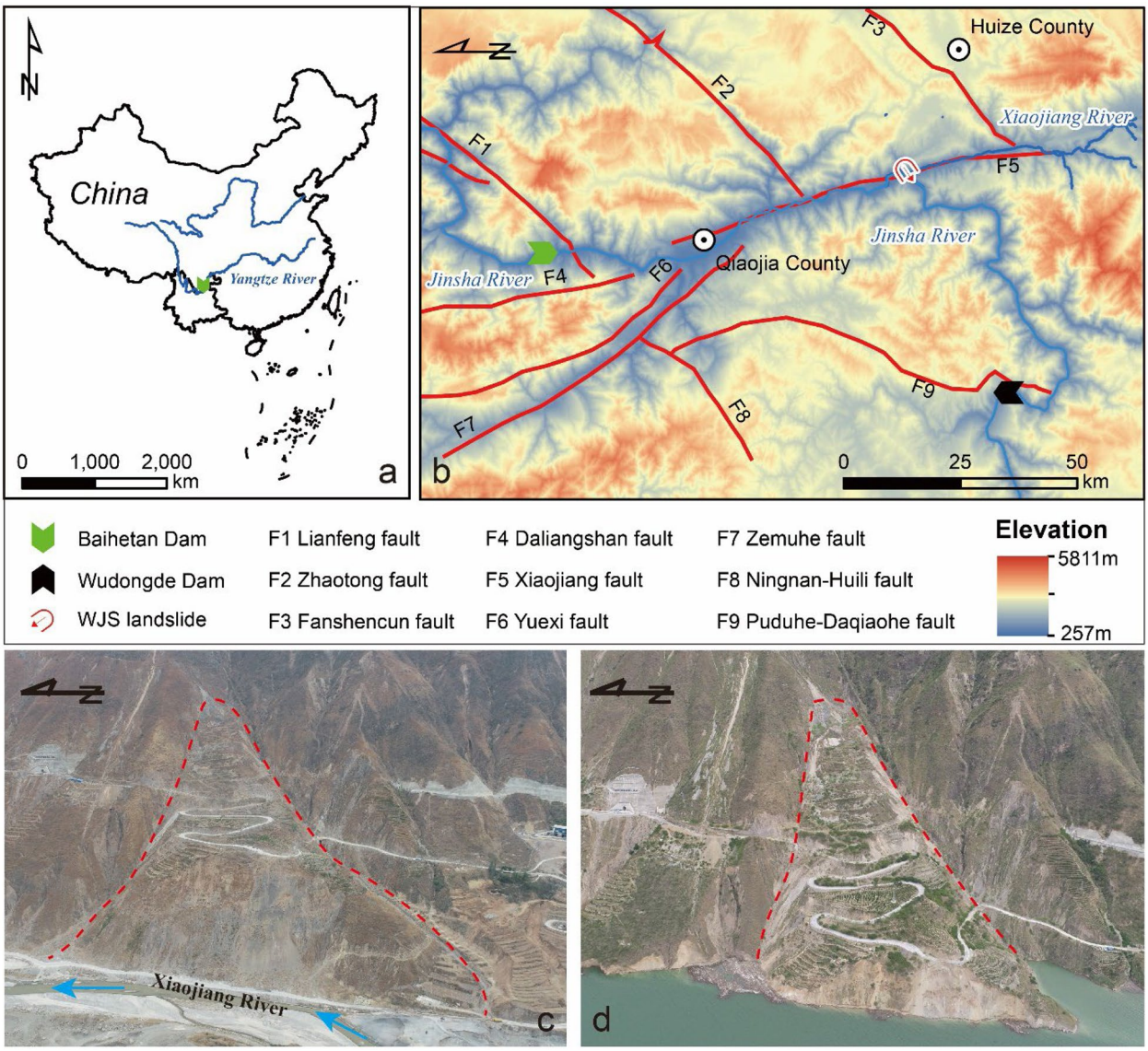

Fig. 1 WJS landslide. **a, b** Location of the WJS landslide; **c** WJS landslide panoramic photograph captured before impoundment (photographed by UAV on March 1, 2021); **d** WJS landslide panoramic photograph captured during the impoundment period (photographed by UAV on October 11, 2021)

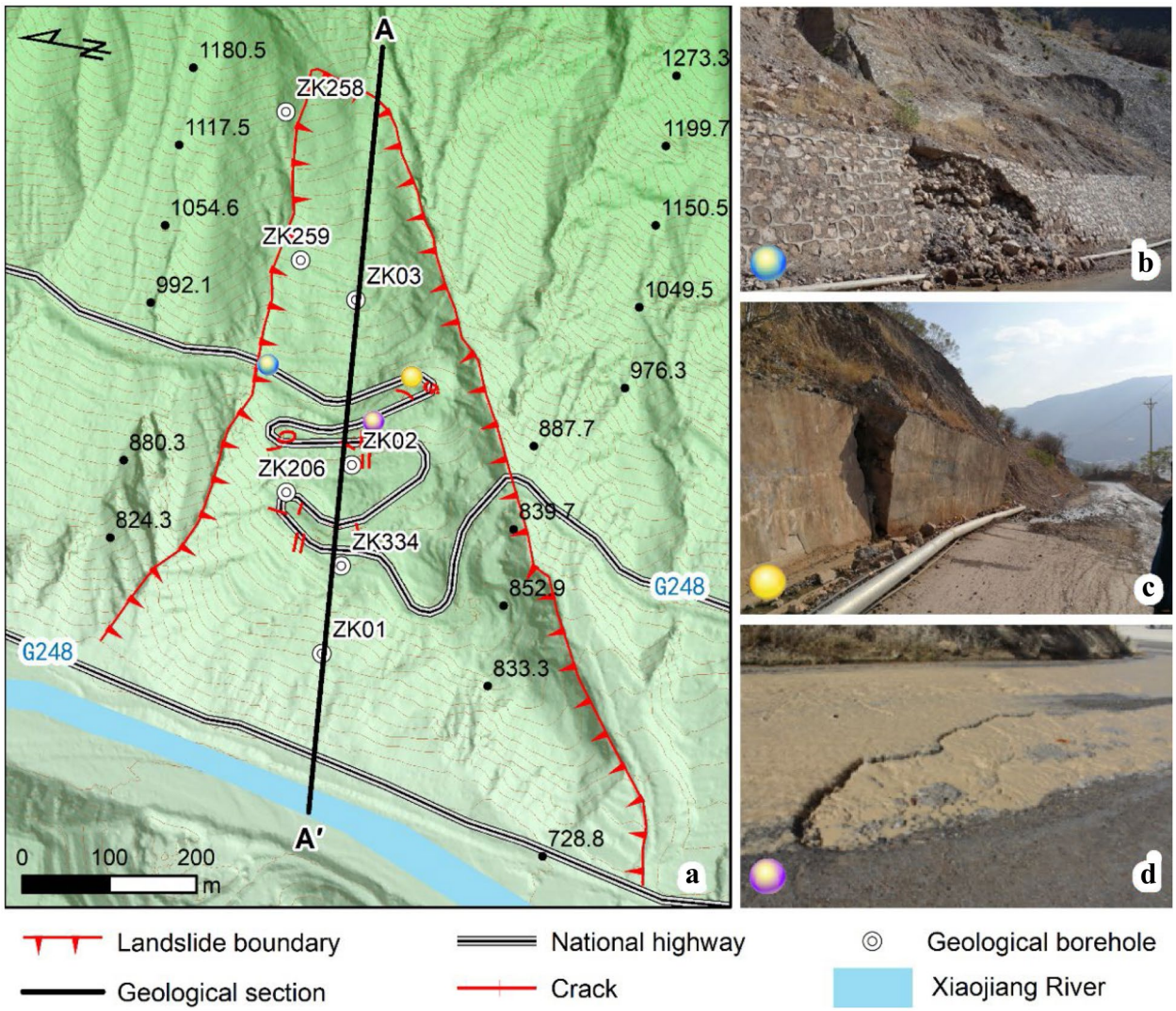

Fig. 2 Planar map of the WJS landslide. **a** Planar map of the WJS landslide; **b** broken retaining wall; **c** toppling of the retaining wall; and **d** tension cracks in the road surface

than the surrounding areas due to river erosion and road excavation. Ditches border both sides of the landslide, and flowing water is present in the rainy season. The ditches converge upward at the back edge. The maximum longitudinal length of the landslide is approximately 800 m, its width is in the range of approximately 90–500 m, its area is approximately 23.5×10^4 m^3, and its estimated volume is 611×10^4 m^3.

Material composition and structural characteristics

The borehole data and field investigation yield the geological profile drawn in Fig. 3. The upper part of the landslide mass is a mixture of displaced rock blocks, gravel, silt, and loose soil and has a thickness of approximately 14.0–49.9 m. The displaced rock blocks are mainly distributed at the back edge of the landslide, resulting from the accumulation of rock crumbling. Sampling statistics at several places along the landslide show that the upper landslide mass contains approximately 10–15% boulders (grain sizes of 0.2–1.0 m), 20–30% gravel (grain sizes of 6–20 cm), and 30–40% gravel (0.5–6 cm), and the rest is silt. According to the Chinese Ministry of Construction of the People's Republic of China (2007), the soil can be classified as gravel mixed soil with a permeability coefficient of $1.85 \times 10^{-3} \sim 1.05 \times 10^{-2}$ cm/s. The lower part of the landslide mass is silty gravel, and it is dark gray with a relatively dense structure. The gravel content is approximately 50–60%, and the rest is silt; the thicknesses are approximately 3.04–13.5 m.

The sliding zone is composed of gravel containing clay; it is grayish-black, with 20–30% gravel content, and the rest is clay. The slip zone is intercalated and distributed within the silty gravel in the lower part of the landslide; it is exposed in ZK01, ZK02, ZK03, and ZK334 but is not obvious in ZK258. According to the borehole data analysis, the sliding zone is chair-shaped and has a thickness of 0.61–2.26 m.

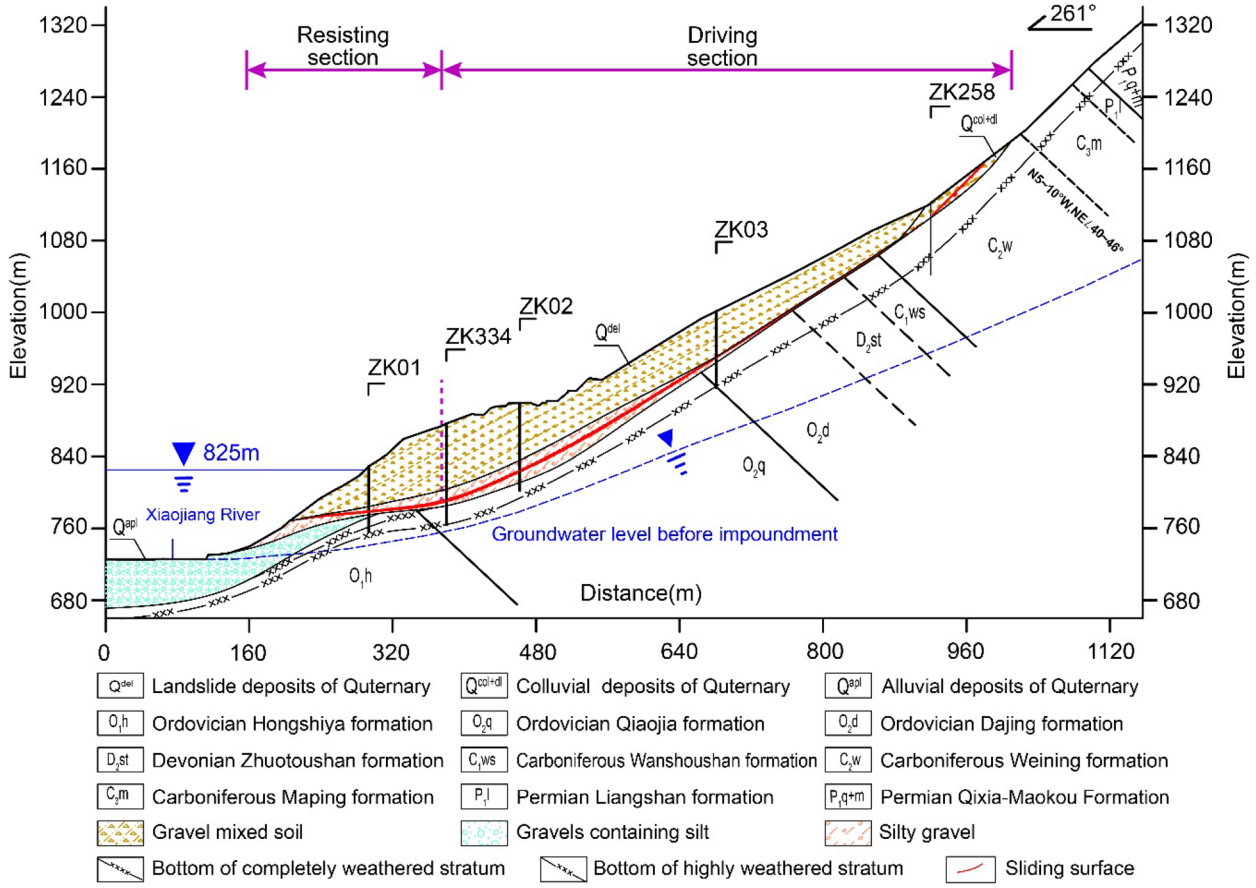

Fig. 3 Longitudinal profile A–A′ of the WJS landslide in Fig. 2

The landslide bed is bedrock composed of Ordovician, Devonian, and Carboniferous limestone, dolomite, and quartz sandstone intercalated with siltstone, mudstone, and shale. The strata are oriented N5-10°W, NE∠40–46°. According to the analysis of the bedrock revealed by the borehole, the landslide bed is affected by the Xiaojiang Fault and river erosion, which has resulted in a high degree of joint fracture development, and the upper part of the landslide bed is highly weathered or completely weathered.

Deformation characteristics before impoundment

In recent years, the InSAR technique has been widely used for deformation analyses of geological hazards such as landslides (Wasowski and Bovenga 2014; Galve et al. 2017; Rosi et al. 2018). In this study, the deformation characteristics of the WJS landslide before impoundment were analyzed using the small baseline subset InSAR technique. The synthetic aperture radar (SAR) satellite data were obtained using 77 scenes from Sentinel-1A descending track data spanning from February 19, 2017, to March 30, 2021. The data were processed, and the obtained WJS landslide displacement rate and cumulative displacement are shown in Figs. 4 and 5, respectively. Figure 4b shows the slope aspect velocity field transformation using the method proposed by Herrera et al. (2013).

As shown in Fig. 4, the mean deformation rate of the WJS landslide in the line-of-sight (LOS) direction ranges from -69 to -14 mm/a, while the mean deformation rate in the slope aspect direction reaches -220 mm/a. The landslide deformation is concentrated within the white dashed circle in the middle area, and the deformation around it gradually decreases outward. In the field survey, deformation phenomena such as broken retaining walls (Fig. 2b), toppled retaining walls (Fig. 2c), and cracked roads (Fig. 2d) were found in the white dashed circle area. Moreover, nine time series cumulative deformation graphs of the WJS landslide were obtained (Fig. 5). The central part of the landslide deformed first and then expanded to the leading and trailing edges, and the cumulative deformation gradually increased. The signs of deformation found in the field investigation are also concentrated in the middle of the landslide (Fig. 2a), which is consistent with the area with the largest cumulative displacement. The above analysis shows that the WJS landslide was undergoing slow deformation before impoundment.

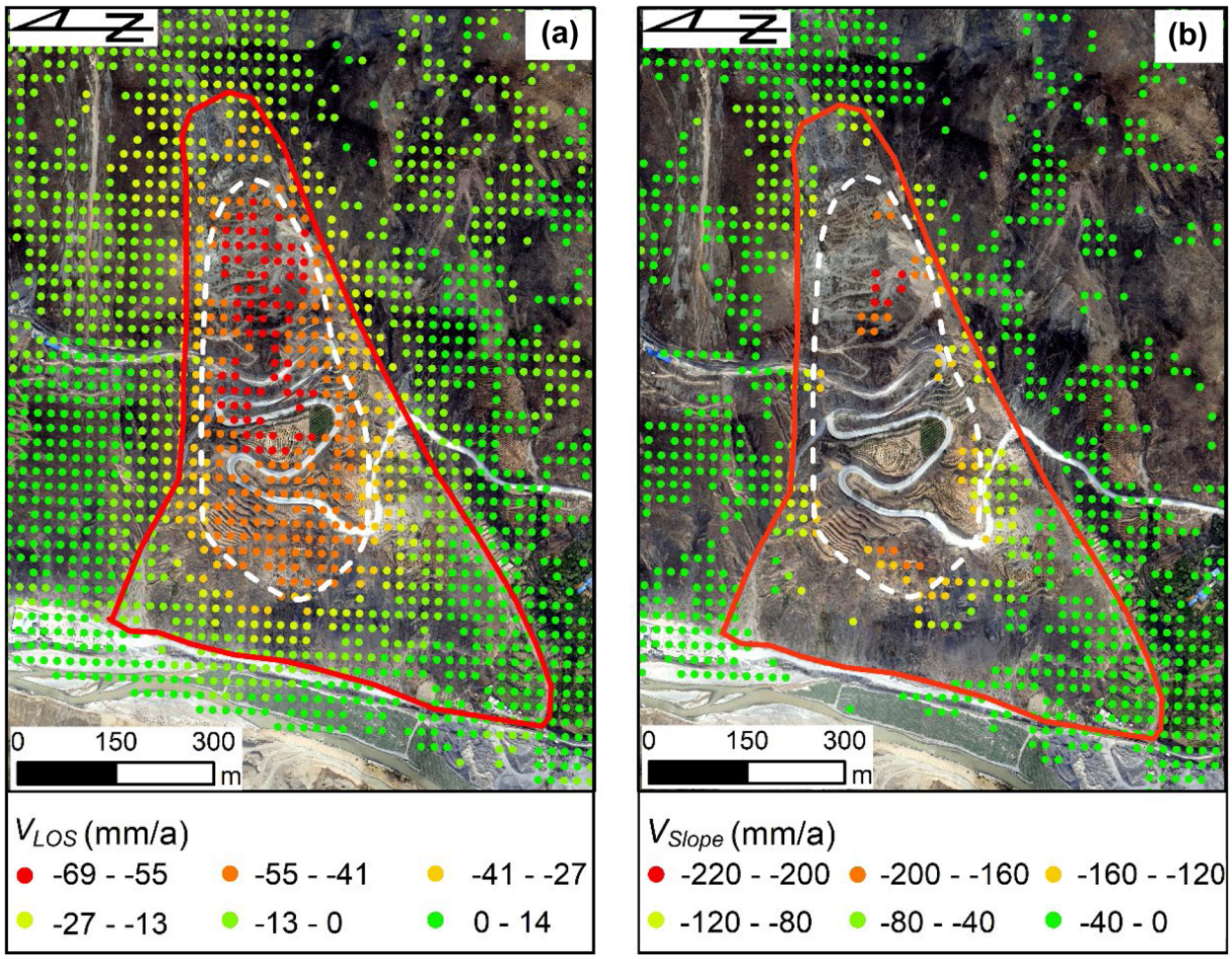

Fig. 4 Mean deformation velocity of the WJS landslide: **a** LOS direction and **b** slope aspect direction

Methodology

To understand the deformation characteristics of the WJS landslide during the impoundment period and to provide reliable data for the early warning of possible rapid landslide events, hydropower plant authorities have installed various monitoring devices on and around the WJS landslide (Fig. 6). These monitoring devices can be classified into three types depending on the recorded information. The first type is equipment that measures environmental parameters, such as rainfall, groundwater level, and reservoir water level. Among them, rainfall is measured by a rain gauge (RG01) installed at the periphery of the right boundary of the WJS landslide, the groundwater level is measured by a vibrating string-type piezometer (PI01) installed in the middle of the landslide, and the reservoir water level is measured by a water level observatory arranged in the Baihetan Reservoir region. The second type is equipment for measuring displacement data, mainly GNSS displacement meters (DP01-DP05) for measuring landslide surface displacement and borehole inclinometers (IN01 and IN02) for measuring deep displacement. The third type includes microcore piles (Fig. 6b) for measuring kinetic data, which are installed on the back edge (MC01) and front edge (MC02) of the landslide and can measure parameters such as azimuth angle and tilt angle (Du et al. 2015; He et al. 2021). In addition, the researchers used a DJI Phantom 4 real-time kinematic (RTK) UAV (Fig. 6c) to collect multiperiod image data of the landslide during the impoundment period. These UAV data were processed using software such as Pix4Dmapper to generate point cloud data of the landslide surface, and comparing the point cloud data over time revealed elevation changes in the landslide (Lucieer et al. 2014; Xu et al. 2020).

Results and analysis

Deformation characteristics during impoundment

The Baihetan Reservoir commenced impoundment on April 6, 2021, and reached its maximum water level of 816.51 m on September 30, before the water level gradually declined and ultimately stabilized at approximately 795 m. Figure 7 depicts the time series displacement curves of the WJS landslide GNSS displacement monitoring stations throughout this timeframe. The displacement monitoring data suggest that the deformation of the WJS landslide was mostly controlled by the variations in reservoir water and that rainfall during the impoundment period did not induce faster deformation of

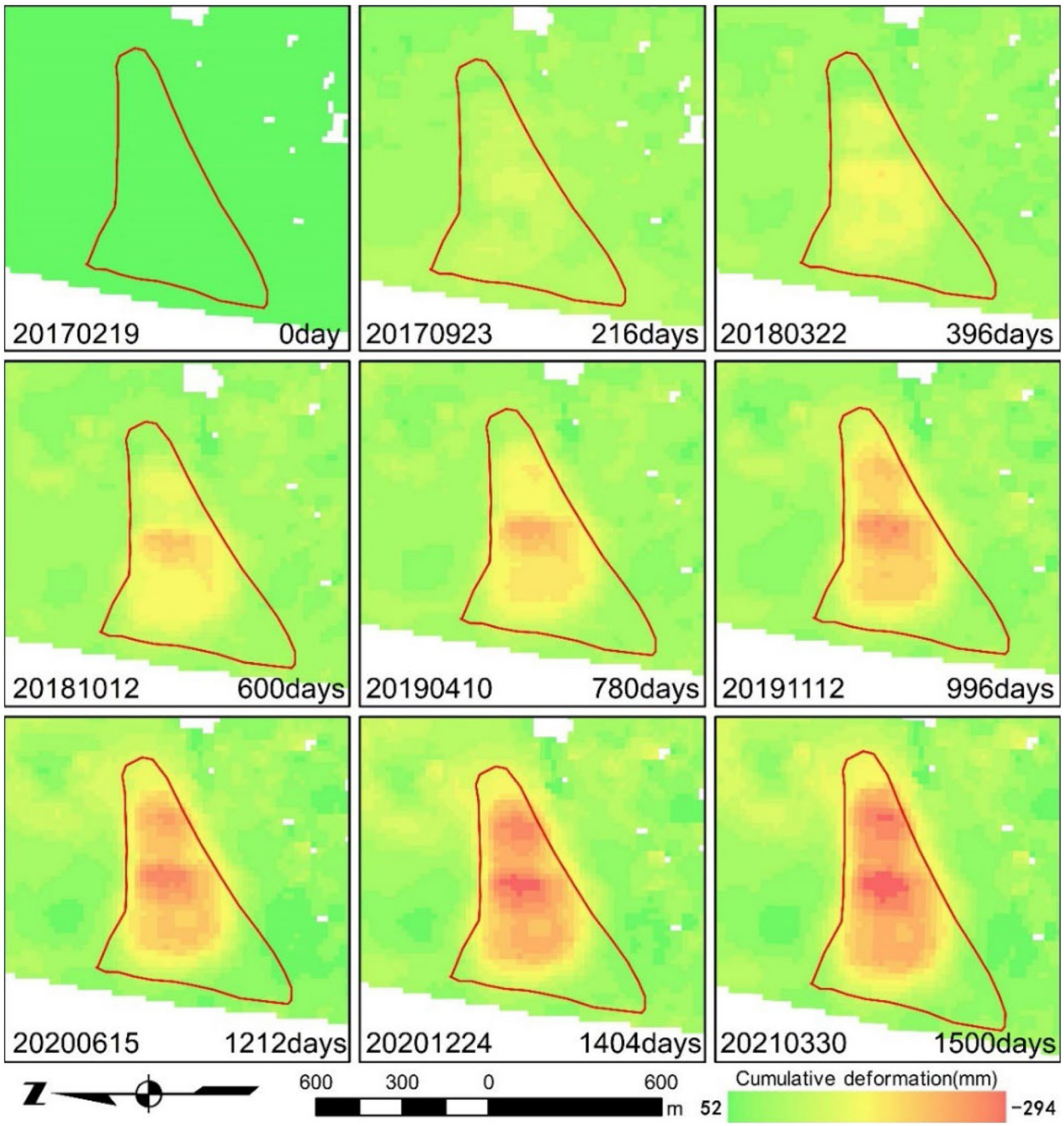

Fig. 5 Time series cumulative deformation maps along the LOS direction from February 19, 2017, to March 30, 2021, with a reference SAR acquisition date of 20,170,219

the WJS landslide. The displacement of the WJS landslide maintained a stable state in the early stages of impoundment but then entered a very rapid deformation state on September 2, and the displacement rate observed by the GNSS station grew significantly.

As the reservoir level rose, the borehole inclinometer monitored sliding along the deep sliding zone of the WJS landslide. The location of the deep sliding surface indicated by the inclinometer was similar to the location of the sliding surface indicated by the prior drilling, as illustrated in Fig. 8. From July 19, 2021, to August 23, 2021, the slip surface at 43.0 m at IN01 moved at a rate of 2.50 mm/day. Before June 27, the slip surface displacement rates at 32.5 m and 75.0 m at IN02 were reasonably constant, with average rates of 0.41 mm/day and -0.02 mm/day, respectively. After June 27, the sliding zone displacement rates at IN02 at depths of 32.5 m and 75.0 m reached 5.33 mm/day and 6.59 mm/day, respectively. These data suggest that the deep slip surface caused a faster sliding rate after the reservoir level reached 780.24 m on June 27.

The deformation of the WJS landslide during the impoundment period is depicted in Fig. 9. The field investigation found that impoundment caused many cracks in the WJS landslide mass

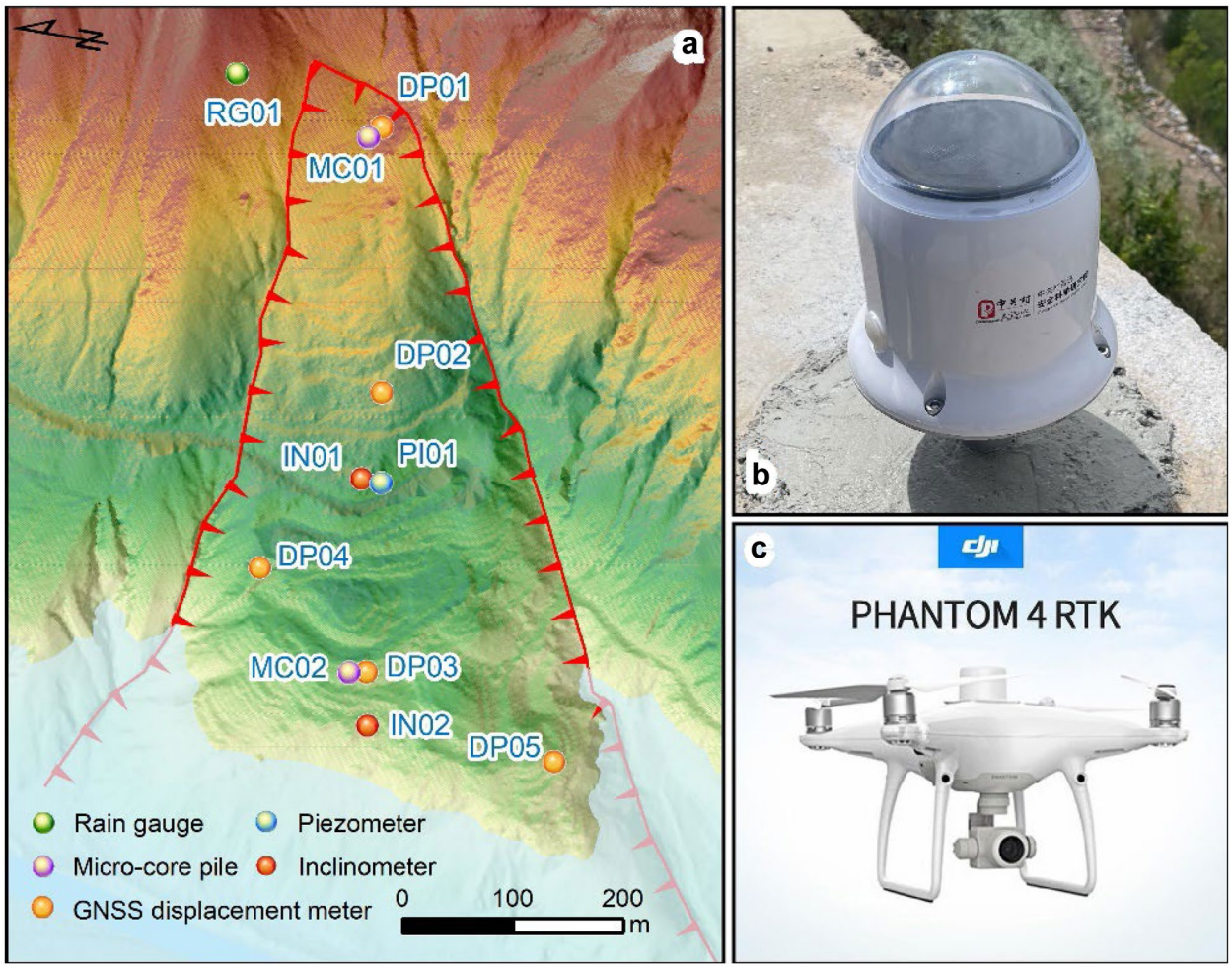

Fig. 6 Monitoring system of the WJS landslide. **a** Location of the automatic monitoring instrument; **b** microcore pile; and **c** DJI Phantom 4 RTK UAV

(Fig. 9a). Furthermore, an arc-shaped scarp with elevation differences of 6.0–9.0 m formed in the head of the landslide, and many transverse tension cracks developed at the lower part (Fig. 9b). Many road cracks formed in the middle and lower regions of the landslide mass, and their orientations were similar to the landslide's sliding direction (Fig. 9c). In the pavement, road deformation (Fig. 9d) and shear dislocation (Fig. 9e) occurred. These observations suggest that when the reservoir water level rose, the landslide slid along the whole sliding zone.

Deformation processes during impoundment

The elevation change in the WJS landslide during the initial impoundment of the Baihetan Reservoir is depicted in Fig. 10. The reservoir water level was 728.75 m on April 28 and had just reached the Xiaojiang River. The reservoir water had little effect on the landslide, and there was no displacement change when compared to the digital elevation model (DEM). The reservoir water level increased and reached 761.49 m on May 25, when only a small-scale bank collapse occurred at the landslide foot (Fig. 10a). The reservoir level then rose quicker, reaching 776.37 m on July 11, and the bank collapse at the landslide foot grew larger (Fig. 10b). The reservoir water level then gradually declined to 771.82 m on August 14, and the bank collapse area increased, but the landslide mass displacement was not visible (Fig. 10c). After the flood season ended, the reservoir water level rose more quickly in September, reaching 801.09 m on September 14, when vertical displacements at the road and the landslide crown were 0–1.0 m (Fig. 10d). On September 30, the reservoir water level reached its highest level of 816.51 m and then gradually decreased. The elevation comparison data between November 4 and April 8 revealed a significant height difference at the landslide head, with displacements ranging from 2.0 to 7.0 m (Fig. 10e). Furthermore, the middle road deformation reached 5.0–8.0 m, and the scope and depth of bank collapse at the landslide foot increased. In November, the reservoir water level dropped to approximately 795 m, the landslide deformation trend slowed, and the deformation degree did not considerably rise (Fig. 10f).

The WJS landslide underwent a complex deformation process during the impoundment period, according to the study of the DEMs recorded by UAV. This process began with a bank collapse at the landslide toe and progressed to sliding of the whole landslide. The deformation process since impoundment on April 6, 2021, was

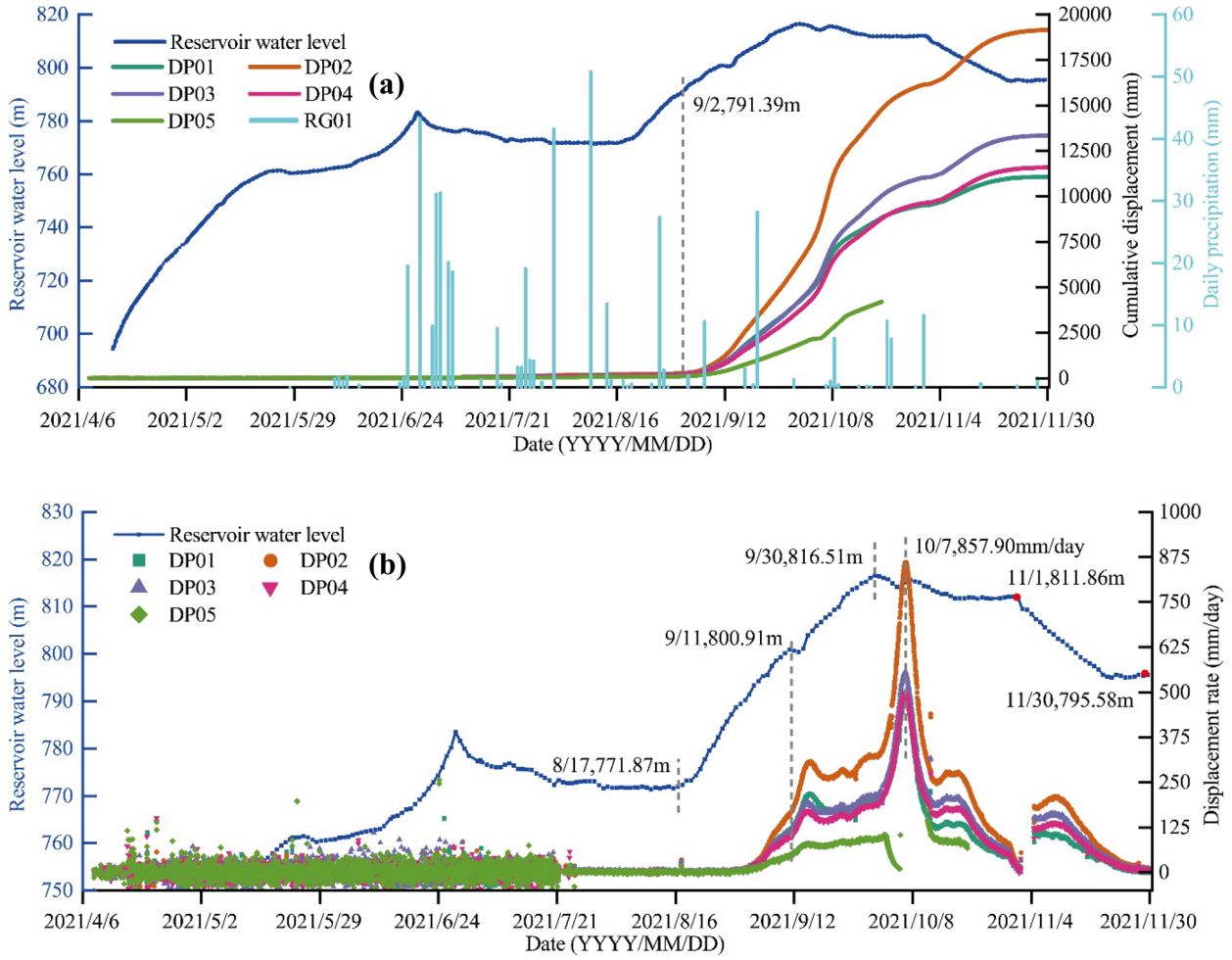

Fig. 7 Time series curves between the displacements measured by several GNSS stations and the reservoir water level and rainfall. **a** Comparison of the cumulative displacement with the reservoir water level and rainfall and **b** comparison of the displacement rate with the reservoir water level

classified into six stages by analyzing multisource monitoring data of the WJS landslide during the impoundment period:

(1) Stage 1 occurred from April 6, 2021, to April 29, 2021. The reservoir water level rose from 660.35 m to 730.13 m at this stage, and the reservoir water level touched the G248 national road at the landslide's front edge. The reservoir water level had little effect on the landslide at this stage, the landslide deformation rate had not changed since before impoundment, and the GNSS displacement monitoring station's deformation rates were 0.02–0.06 mm/day.

(2) Stage 2 occurred from April 30, 2021, to June 9, 2021. During this phase, the reservoir water level rose from 730.13 m to 762.65 m, causing bank collapse near the landslide foot (Fig. 10a). The GNSS sites (DP03, DP04, and DP05) near the leading landslide foot had substantial oscillations in their vertical displacement curves, resulting in a much higher vertical settlement deformation than horizontal displacement (Fig. 11).

(3) The third stage occurred from June 10, 2021, to July 6, 2021. The reservoir level rose to 783.49 m during this period and then fell to 776.28 m. The sliding zone at the landslide foot (768.42 m) was submerged by reservoir water when the reservoir water level rose. On June 10 and June 27, the MC02 microcore piles measured a change in tilt angle and azimuth angle at the landslide foot (Fig. 12), and on June 27, the IN02 inclinometer assessed the abrupt change in displacement at the deep sliding zone (Fig. 8d). The bank collapse near the landslide foot was further expanded, according to the UAV images (Fig. 10b). Except for that at DP01, the horizontal displacement rates rose during this time at the other GNSS stations, reaching 1.1 mm/day. These observations suggest that the shear strength of the sliding zone near the landslide toe gradually decreased as reservoir water acted on it, and the landslide showed creep-slip deformation along the deep sliding zone. The DP01 monitoring station at the landslide head had a smooth horizontal cumulative displacement curve that did not follow the same trend as the other stations (Fig. 13). This indicates that the WJS landslide had not yet undergone overall sliding.

(4) Phase 4 occurred from July 7, 2021, to September 1, 2021. As the reservoir level changed, the accumulated displacement of the DP01 monitoring station changed abruptly and started to increase linearly on July 7 after a long period of stability (Fig. 13). The MC01 microcore pile measured an increase in the tilt angle on July 10,

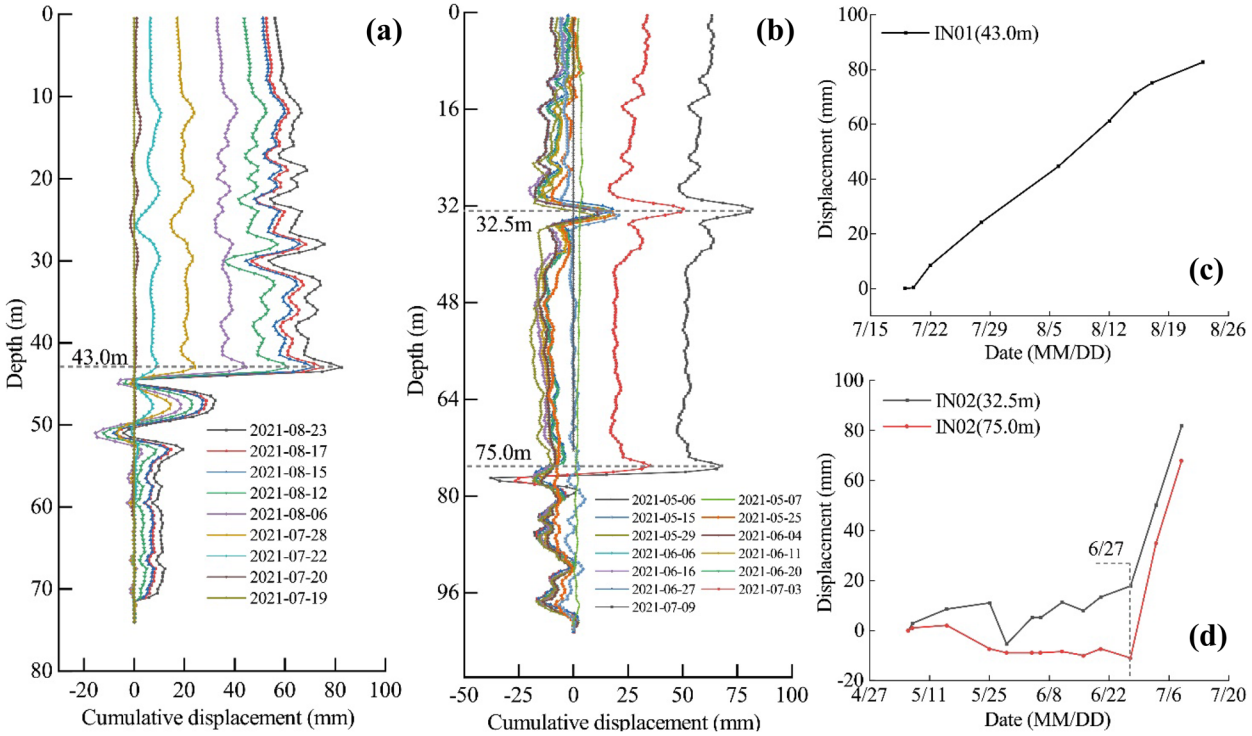

Fig. 8 Displacement data measured by borehole inclinometers. **a** Displacement curve of IN01; **b** displacement curve of IN02; and **c** and **d** time series of sliding zone displacement measured by inclinometers at different depths

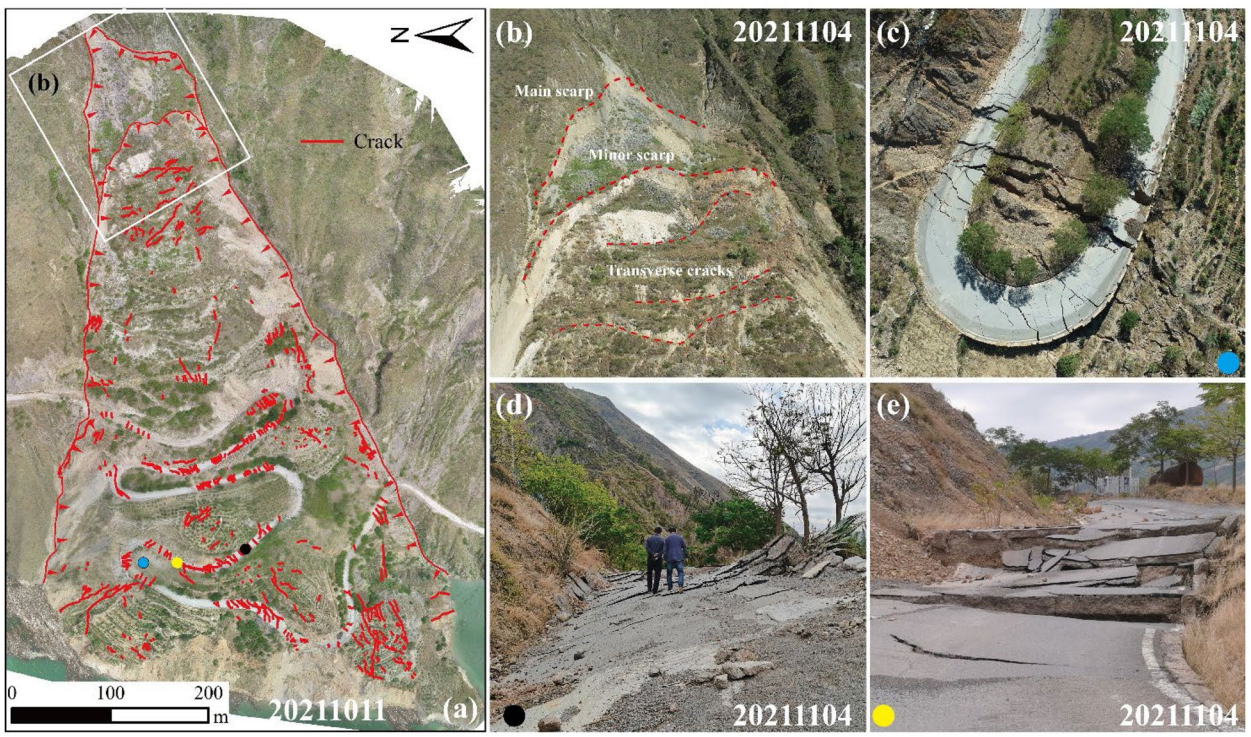

Fig. 9 Deformation characteristics of the WJS landslide during impoundment. The blue, black, and yellow dots in Fig. 9a indicate the locations of photographs in Fig. 9c–e. **a** Cracks in the landslide; **b** tension scarps and transverse cracks in the head of the landslide; **c** road cracks; **d** transverse ridges; and **e** damaged roads

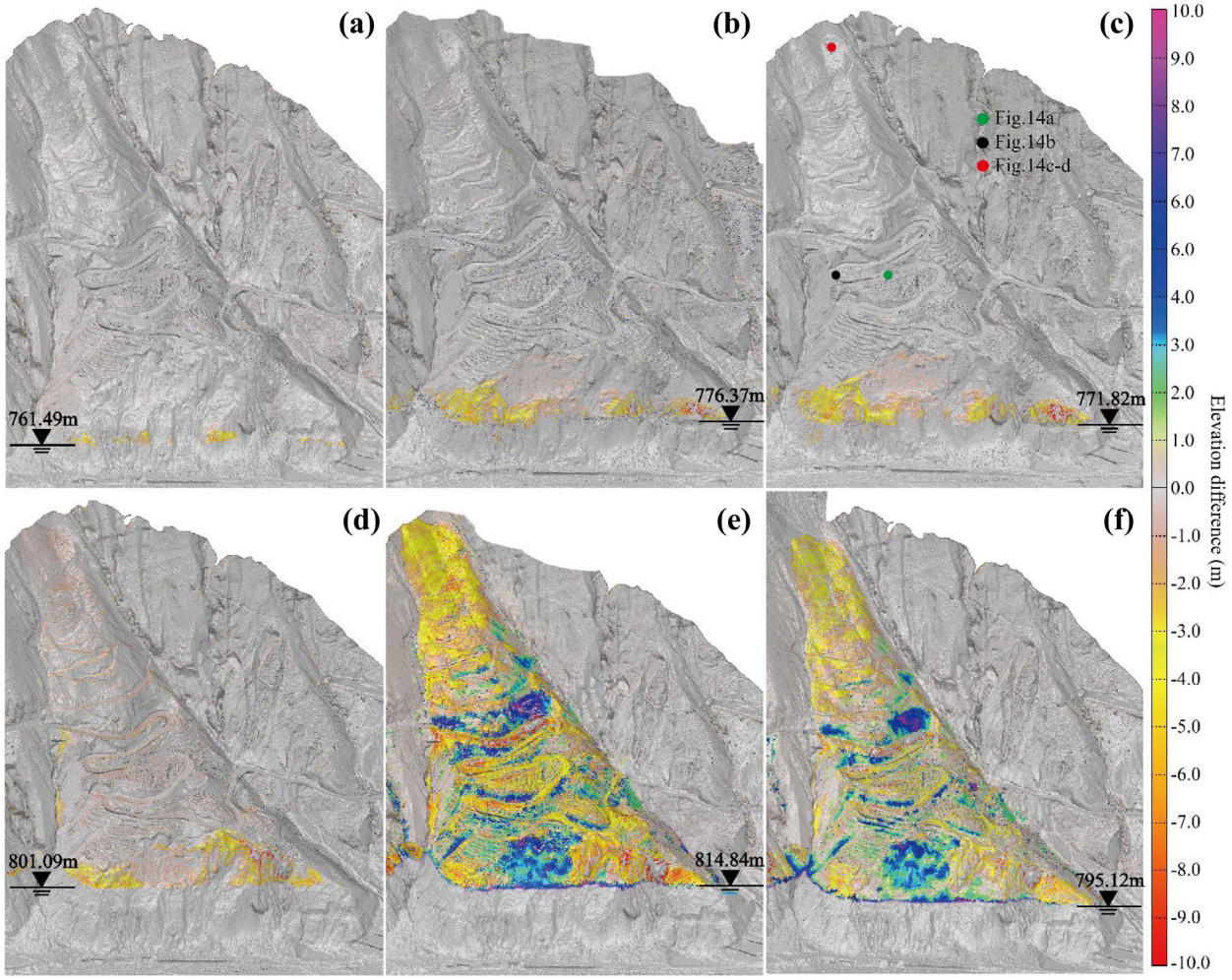

Fig. 10 Change in the WJS landslide elevation during the impoundment period based on UAV data acquired on 20,210,408. Positive and negative values indicate elevation increases and decreases, respectively. **a** 20,210,525; **b** 20,210,711; **c** 20,210,814; **d** 20,210,914; **e** 20,211,104; and **f** 20,111,121

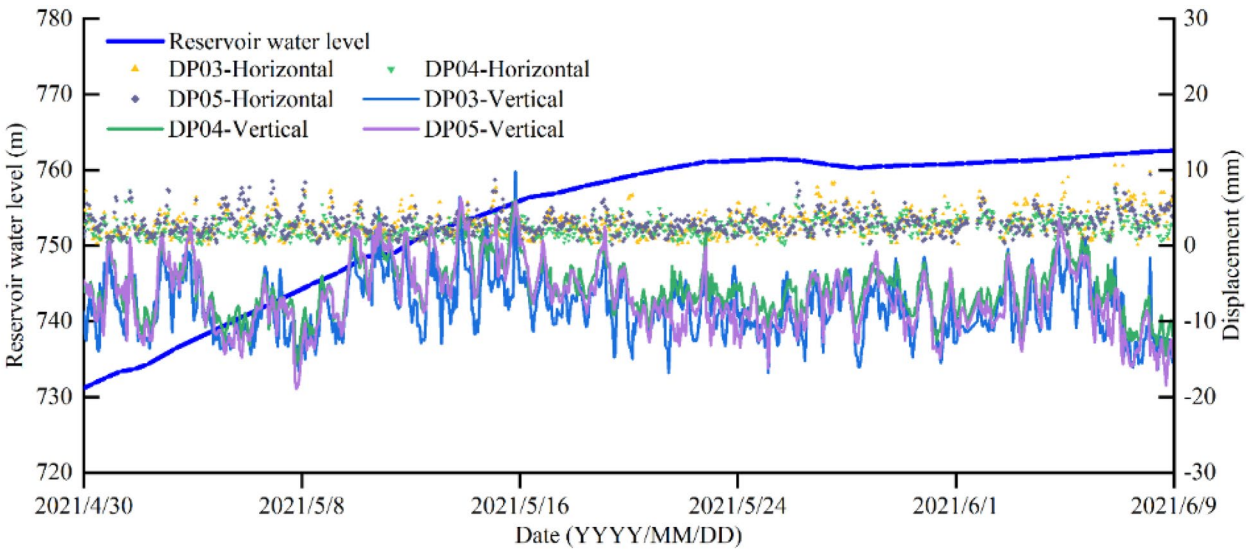

Fig. 11 Cumulative horizontal and vertical displacements measured by the DP03, DP04, and DP04 GNSS stations from April 30, 2021, to June 9, 2021

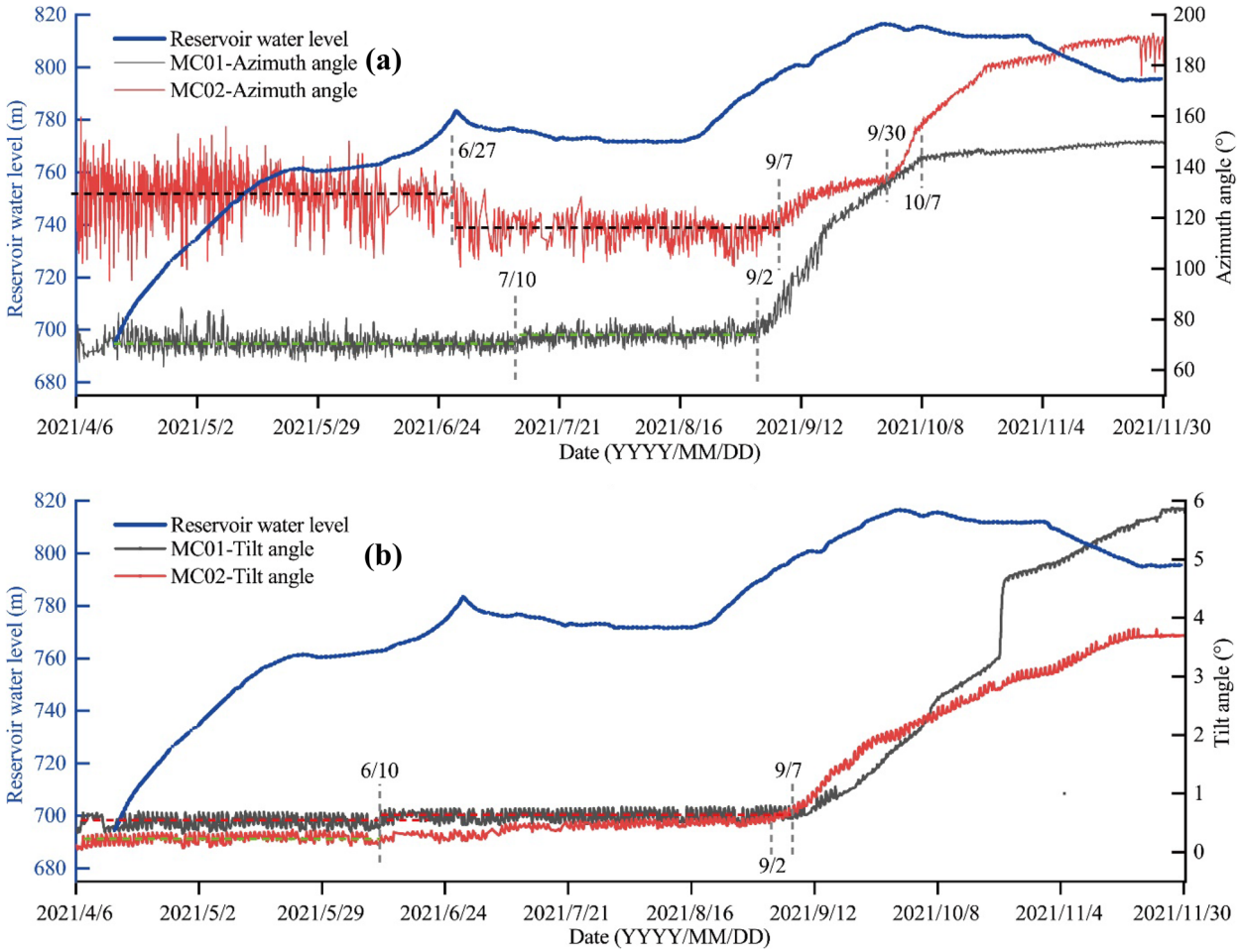

Fig. 12 Variation in the azimuth and tilt angle of the microcore piles corresponding to the reservoir water level. **a** Azimuth angle and **b** tilt angle

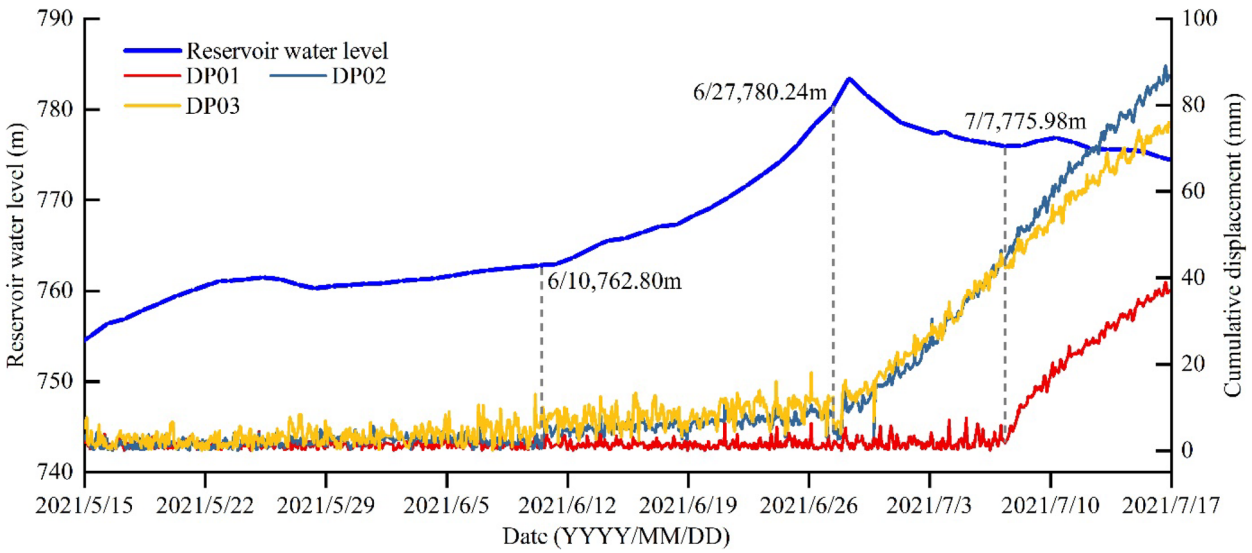

Fig. 13 Time series displacement curves measured at the DP01, DP02, and DP03 GNSS stations (May 15, 2021, to July 17, 2021)

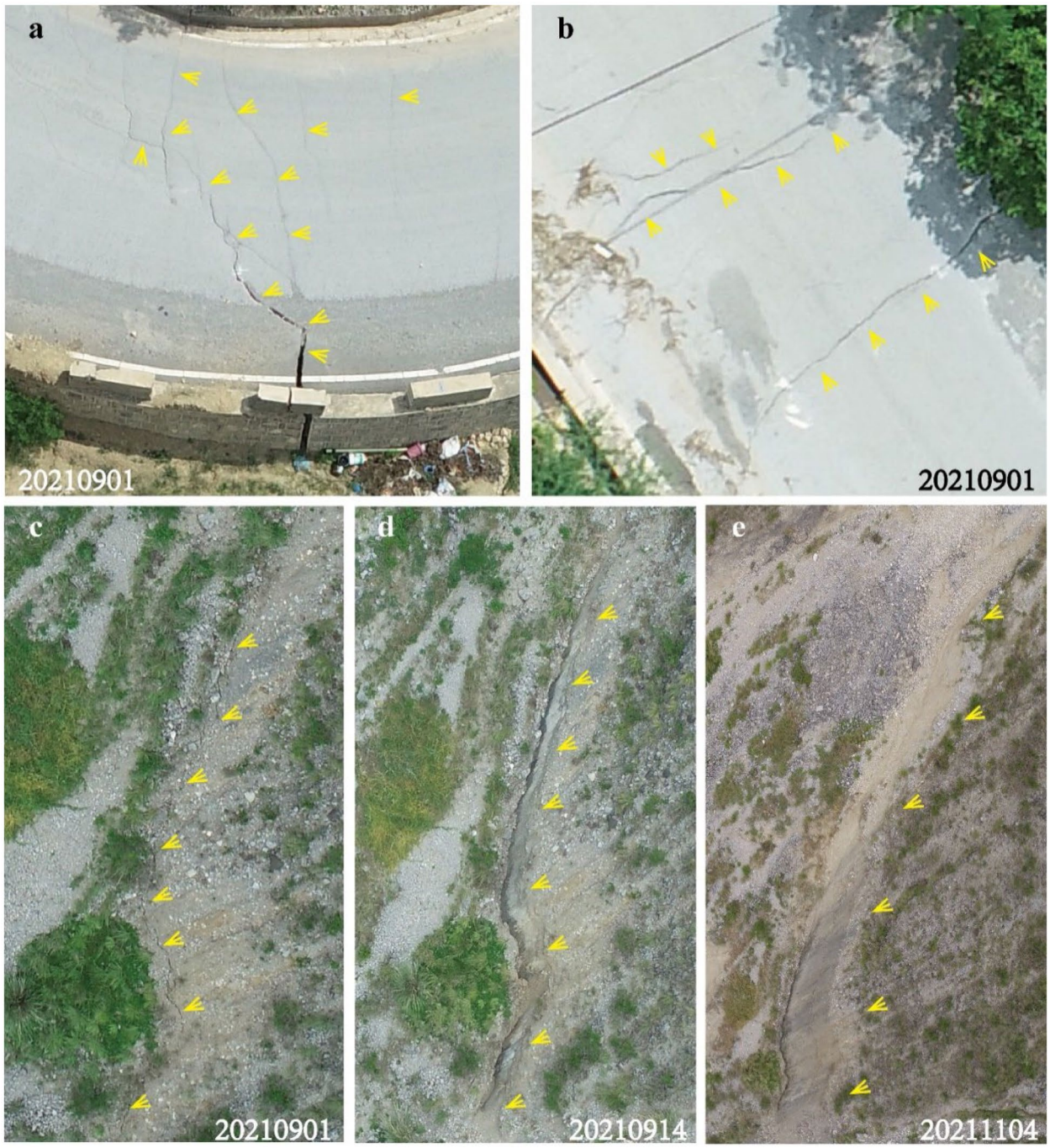

Fig. 14 Deformation characteristics of the WJS landslide. **a** and **b** Cracks in the road; **c–d** shear crack at the left boundary of the landslide crown

the MC02 microcore pile measured a slow increase in the tilt angle (Fig. 12b), and the inclinometer in the middle of the slide measured a deep slide surface displacement rate of 2.50 mm/day (Fig. 8c). During this period, the bank collapse at the landslide foot was further expanded (Fig. 10c and d), longitudinal cracks appeared in the central road (Fig. 14a and b), and small shear cracks appeared at the left boundary of the landslide crown (Fig. 14c). These phenomena indicate that the WJS landslide experienced an overall retrogressive motion during this period, with horizontal deformation rates reaching 1.28–4.15 mm/day.

(5) Phase 5 occurred from September 2, 2021, to October 31, 2021. At this stage, the reservoir water level rose to 816.61 and then decreased slowly to approximately 811 m. During this period, the cumulative horizontal displacement of the GNSS monitoring stations increased rapidly, reaching 9509.81–16,124.80 mm (Fig. 7a), and the average deformation rate of the monitoring stations also

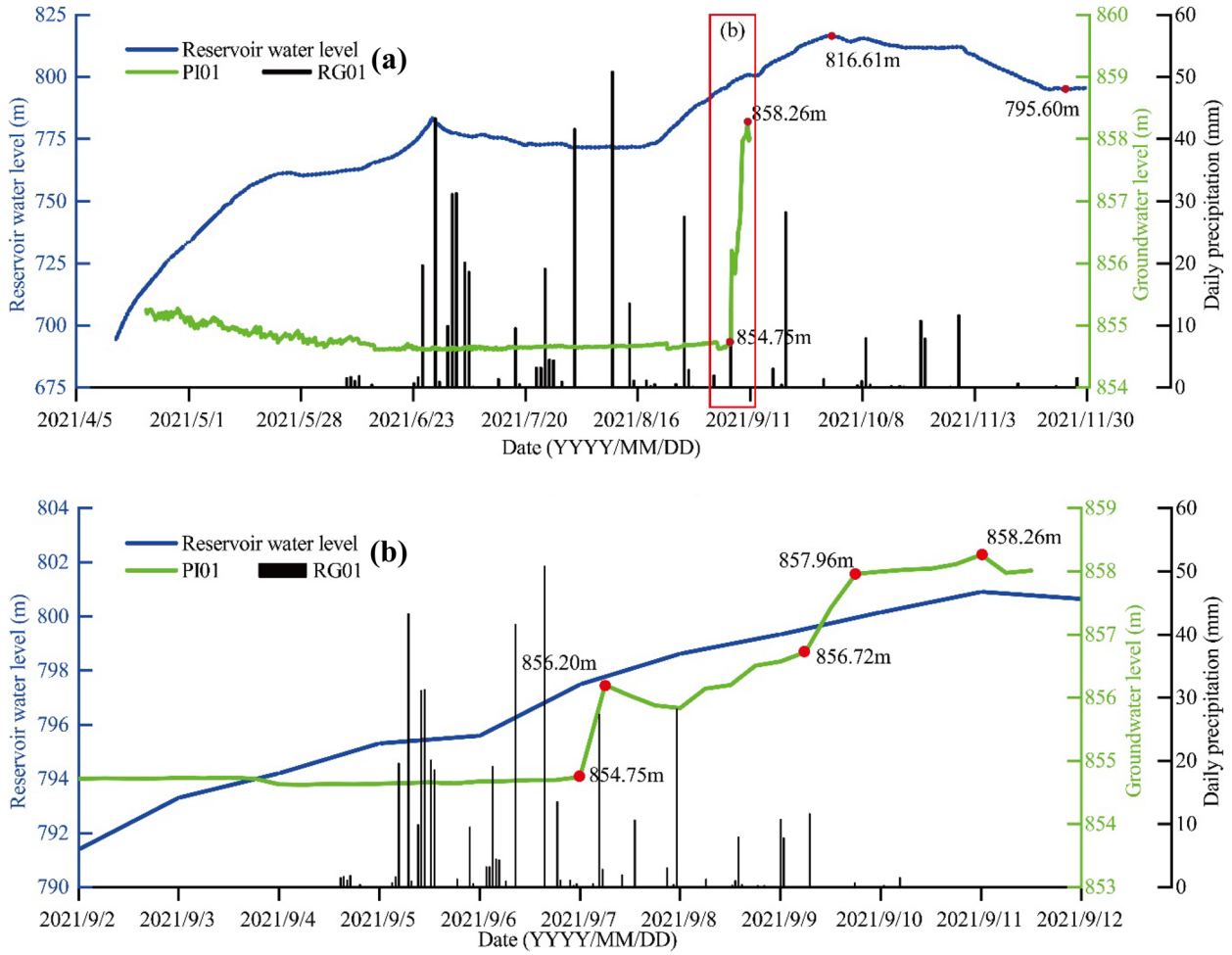

Fig. 15 Diagram comparing reservoir water level, daily precipitation, and groundwater level. **a** 20,210,406–20,211,030 and **b** enlargement of the period 20,210,902–20,210,912 in (a)

reached 150–300 mm/d. The azimuth and tilt angle parameters also changed dramatically because of the rapid increase in the landslide deformation rate (Fig. 12). The groundwater level, which remained stable (854.75 m) as measured by piezometer PI01, increased significantly and reached 858.26 m on September 11, 2021, with an increase of 3.51 m (Fig. 15). Then, the piezometer could not obtain data because the connecting cable was cut off due to excessive deep shear deformation. On October 7, the horizontal displacement rate of the monitoring station reached its maximum, where the DP02 deformation rate was 857.90 mm/day, lagging behind the highest reservoir level by approximately seven days (Fig. 7). At this stage, because of the integral sliding of the landslide, shear cracks penetrated the left boundary of the landslide crown (Fig. 14d, c, and e), and cracks and bulging deformations appeared extensively in the landslide (Fig. 9). These observations show that the landslide slid along the whole sliding zone as the reservoir level rose.

(6) Phase 6 occurred from November 1, 2021, to November 31, 2021. In this stage, the reservoir level decreased from approximately 811 m to 795 m. The decrease in the reservoir level led to an increase in the landslide deformation rate, but it was much smaller than the deformation rate in the period when the reservoir level rose to the high reservoir level (phase 5). Moreover, the deformation rate of the landslide decreased to approximately 2.4–7.8 mm/day when the reservoir level stabilized at 795 m (Fig. 7b). This indicates that the rising reservoir water level accelerated the deformation of the WJS landslide, whereas the decreasing reservoir water level facilitated the stability of the landslide (Fig. 10f).

Discussion

As shown in Fig. 3, the sliding surface of the WJS landslide is chair-shaped, with a gentle sliding surface at the front and a high slope at the middle and rear. The front part has a relatively gentle sliding surface slope but greater landslide mass thickness. It provides the main resistance force for the whole landslide mass and is the resisting section of the landslide. The middle and rear parts have high sliding surface slopes, and the landslide mass slides down along the sliding zone under the action of gravity, which constitutes the driving section of the WJS landslide (Tang et al. 2019b; Zou et al. 2021; Yi et al. 2021). The existence of the resisting section causes the resistance force and the sliding force to be in dynamic equilibrium, which places the WJS landslide in a slow deformation state before impoundment.

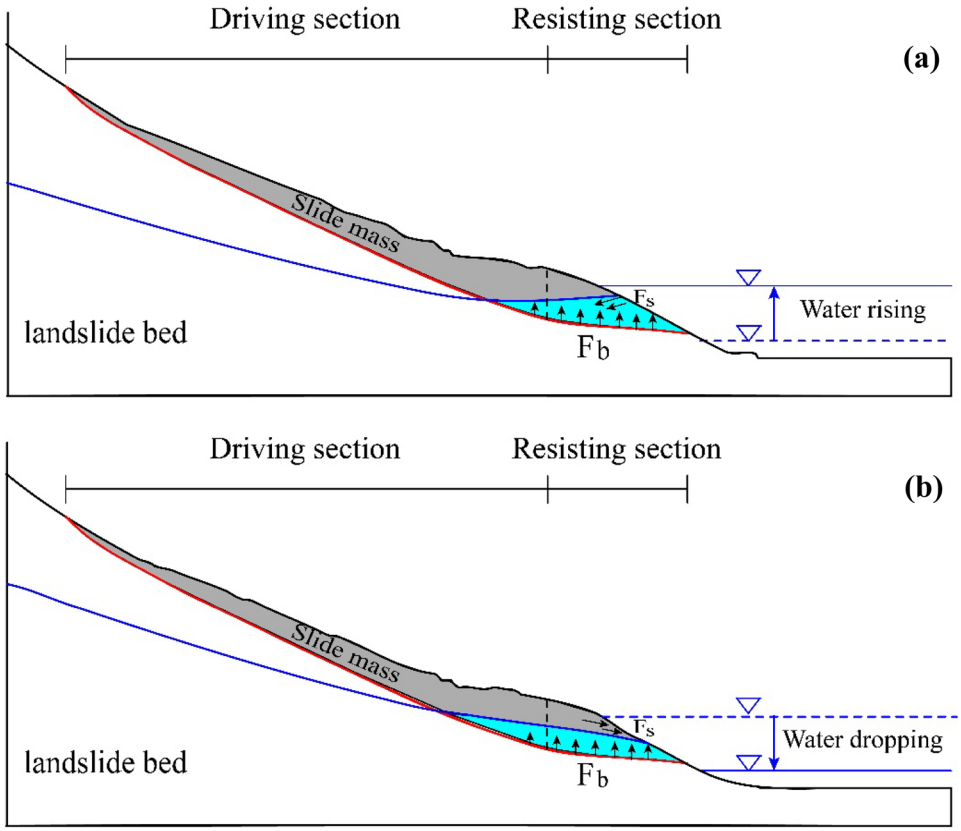

Fig. 16 Deformation mechanism of the WJS landslides. **a** Reservoir water level rise and **b** reservoir water level drop

At the initial stage of impoundment, the soil of the landslide toe lost its structure and strength when encountering water, and local bank collapse occurred. As the water level rose, the reservoir water level reached the elevation of the sliding zone at the front of the landslide on June 20. The influence of reservoir water reduces the shear strength of the WJS landslide sliding zone. As a result, the landslide began to deform under the effect of impoundment, and the IN02 inclinometer also measured the sudden change in the displacement of the deep slip zone on June 27 (Fig. 8d). With the initial impoundment process in the Baihetan Reservoir region, this dynamic equilibrium was broken, which eventually led to the rapid deformation of the WJS landslide.

For landslides partially submerged by reservoir water, the forces acting on the landslide mainly include hydrostatic pressure and hydrodynamic pressure, which are usually expressed in the form of buoyancy force (F_b) and seepage force (F_s) (Wang et al. 2018; Huang et al. 2020; Zou et al. 2021) (Fig. 16). The seepage force (F_s) is a volumetric force whose magnitude is proportional to the hydraulic gradient and whose direction coincides with the seepage direction. When the reservoir level decreases, the outward seepage force decreases the stability of the slope. In contrast, the seepage force is directed inward during the rise of the reservoir water level, thus increasing the slope stability. The buoyancy force (F_b) occurs when the sliding mass immersed in the reservoir water is lifted vertically by the reservoir water. The buoyancy force (F_b) will reduce the effective gravity of the sliding mass and will have opposite impacts on the stability of the landslide when it acts on the resisting and driving sections.

The loose deposits in the WJS landslide are poorly graded and have a large permeability coefficient ($1.85\times10^{-3}\sim1.05\times10^{-2}$ cm/s). This is lower than the daily rising rate of reservoir water, resulting in waterhead differences inside and outside the landslide mass. As the reservoir water level continues to rise, the seepage volume of the landslide foot gradually increases. When the reservoir water rises to the front edge of the landslide and infiltrates into the slope, the sliding mass is subjected to the buoyancy force of the reservoir water, forming the buoyancy weight-reducing effect. The buoyancy weight-reducing effect leads to a decrease in the normal stress on the sliding surface, a decrease in the resisting force of the landslide, a decrease in the overall stability, and a high-speed deformation at high water levels (Fig. 16a). Since the permeability coefficient of the landslide mass is smaller than the daily rise in the reservoir water level, the WJS landslide reaches the maximum deformation rate at a lag of seven days (Fig. 16b). Then, the water level in the Baihetan Reservoir region gradually decreases from the highest level in the initial impoundment period and stabilizes at approximately 811 m, the groundwater levels inside and outside the slope gradually balance, and the seepage pressure gradually decreases. At this stage, part of the buoyancy force acts on the driving section, and the sliding force is reduced to a certain extent. As the reservoir water level decreases, the buoyancy force also decreases, resulting in a rise in the resisting force compared with the high water level. The landslide stability increases, and the deformation rate is reduced by adjusting the sliding forces and resisting forces at this stage.

The water level in the Baihetan Reservoir region will gradually decrease to 765 m by the end of May 2022. According to the analysis

of the initial water storage deformation mechanism of the WJS landslide, the stability of the landslide will gradually increase when the water level drops due to the dissipation of the buoyancy effect and the increase in the resisting force (Fig. 16b). However, when the reservoir water drops rapidly, the landslide will be subjected to seepage pressure in the sliding direction due to the waterhead differences inside and outside the landslide mass, and the deformation rate will increase (Fig. 16b). In general, the buoyancy weight-reducing effect has a more significant impact on the stability of the WJS landslide. The stability reaches the lowest value during the impoundment period, while the probability of large-scale sliding in the discharge period is low.

Conclusions

This paper analyzes the deformation characteristics and mechanism of the WJS landslide in the Baihetan Reservoir region during the initial impoundment period. The WJS ancient landslide was in a slow deformation state before impoundment, and the impoundment in the Baihetan Reservoir region exacerbated the deformation of the WJS landslide. After the reservoir water level reached the road at the landslide toe, bank collapse of the WJS landslide occurred first, and the scope of the collapse continued to expand with the rise in the reservoir water level. After the reservoir water flooded the front sliding surface of the WJS landslide, the landslide began to creep along the original sliding zone, which developed into overall sliding on July 7. After that, the further rise in the reservoir water level led to rapid sliding after September 2.

The sliding surface of the WJS landslide is chair-shaped, the front part of the landslide mass is the resisting section, and the middle and rear parts comprise the driving section. Because the resisting force and the sliding force are in dynamic equilibrium, the WJS landslide was in a slow deformation state before impoundment. With the gradual increase in the reservoir water level, the buoyancy force of the reservoir water on the landslide mass in the resisting section increased gradually, resulting in a decrease in the normal stress on the sliding surface and a decrease in the resisting force, causing the landslide to slide rapidly. When the reservoir water level dropped from the highest water level and stabilized at approximately 811 m, the groundwater levels inside and outside the slope gradually balanced, and the seepage pressure decreased. A part of the buoyancy force acted on the driving section, which reduced the sliding force and increased the stability of the landslide.

According to the operation plan of the Baihetan Reservoir region, the water level will be gradually lowered to 765 m. As the water level decreases, the buoyancy weight-reducing effect of the reservoir water dissipates, and the landslide stability will gradually increase. The probability of large-scale sliding of the WJS landslide is low. However, monitoring of the WJS landslide needs to be strengthened to study its deformation mechanism at depth.

Conflict of interest

The authors declare that they have no known competing financial interests or personal relationships that could have appeared to influence the work reported in this paper.

Acknowledgements

The authors thank Baoguo Yin, Jingnan Han, Yuting Ren, Zhenghai Xue, and Xian Shan for their help in UAV image acquisition and data processing. We also thank the anonymous referees and the editor for their constructive feedback and suggestions that encouraged us to improve the quality of this paper.

Funding

This research was funded by the National Natural Science Foundation of China (Grant No. 41977252), the National Key Research and Development Program of China (Grant No. 2018YFC1505503), the State Key Laboratory of Geohazard Prevention and Geoenvironment Protection Independent Research Project (Grant No. SKLGP2020Z001), and the Scientific Research Project of Zhejiang Huadong Construction Engineering Co., Ltd. (Grant No. KY2020-HDJS-19).

References

Dun J, Feng W, Yi X et al (2021) Detection and Mapping of Active Landslides before Impoundment in the Baihetan Reservoir Area (China) Based on the Time-Series InSAR Method. Remote Sens 13:3213. https://doi.org/10.3390/rs13163213

Du Y, Xie M, Jiang Y, Li B, Gao Y (2015) Methods for determining early warning indices Based on natural frequency monitoring. Rock Soil Mech 36(08):2284–2290. https://doi.org/10.16285/j.rsm.2015.08.022. (in Chinese)

Galve J, Pérez-Peña J, Azañón J et al (2017) Evaluation of the SBAS InSAR Service of the European Space Agency's Geohazard Exploitation Platform (GEP). Remote Sens 9:1291. https://doi.org/10.3390/rs9121291

He Z, Xie M, Huang Z et al (2021) Method to Realize the Tilt Monitoring and Instability Prediction of Hazardous Rock on Slopes. Adv Civ Eng 2021:1–14. https://doi.org/10.1155/2021/9965113

Herrera G, Gutiérrez F, García-Davalillo JC et al (2013) Multi-sensor advanced DInSAR monitoring of very slow landslides: The Tena Valley case study (Central Spanish Pyrenees). Remote Sens Environ 128:31–43. https://doi.org/10.1016/j.rse.2012.09.020

Huang X, Guo F, Deng M et al (2020) Understanding the deformation mechanism and threshold reservoir level of the floating weight-reducing landslide in the Three Gorges Reservoir Area, China. Landslides 17:2879–2894. https://doi.org/10.1007/s10346-020-01435-1

Li S, Xu Q, Tang M et al (2020) Centrifuge Modeling and the Analysis of Ancient Landslides Subjected to Reservoir Water Level Fluctuation. Sustainability 12:2092. https://doi.org/10.3390/su12052092

Lucieer A, de Jong SM, Turner D (2014) Mapping landslide displacements using Structure from Motion (SfM) and image correlation of multi-temporal UAV photography. Prog Phys Geogr Earth Environ 38:97–116. https://doi.org/10.1177/0309133313515293

Ministry of Construction of the People's Republic of China (2007) Standard for engineering classification of soil (GB/T 50145–2007). China Planning Press, Beijing. (in Chinese)

Pinyol NM, Alonso EE, Corominas J, Moya J (2012) Canelles landslide: modelling rapid drawdown and fast potential sliding. Landslides 9:33–51. https://doi.org/10.1007/s10346-011-0264-x

Rosi A, Tofani V, Tanteri L et al (2018) The new landslide inventory of Tuscany (Italy) updated with PS-InSAR: geomorphological features and landslide distribution. Landslides 15:5–19. https://doi.org/10.1007/s10346-017-0861-4

Semenza E, Ghirotti M (2000) History of the 1963 Vaiont slide: the importance of geological factors. Bull Eng Geol Env 59:87–97. https://doi.org/10.1007/s100640000067

Tang H, Wasowski J, Juang CH (2019a) Geohazards in the three Gorges Reservoir Area, China – Lessons learned from decades of research. Eng Geol 261:105267. https://doi.org/10.1016/j.enggeo.2019.105267

Tang M, Xu Q, Yang H et al (2019b) Activity law and hydraulics mechanism of landslides with different sliding surface and permeability in the Three Gorges Reservoir Area, China. Eng Geol 260:105212. https://doi.org/10.1016/j.enggeo.2019.105212

Wang F, Zhang Y, Huo Z et al (2008) Mechanism for the rapid motion of the Qianjiangping landslide during reactivation by the first impoundment of the Three Gorges Dam reservoir, China. Landslides 5:379–386. https://doi.org/10.1007/s10346-008-0130-7

Wang F-W, Zhang Y-M, Huo Z-T et al (2004) The July 14, 2003 Qianjiangping landslide, Three Gorges Reservoir, China. Landslides 1. https://doi.org/10.1007/s10346-004-0020-6

Wang Y, Yu L, Yin T et al (2018) Stability Analysis of Partially Submerged Landslide with the Consideration of the Relationship between Porewater Pressure and Seepage Force. Geofluids 2018:1–9. https://doi.org/10.1155/2018/9145830

Wasowski J, Bovenga F (2014) Investigating landslides and unstable slopes with satellite Multi Temporal Interferometry: Current issues and future perspectives. Eng Geol 174:103–138. https://doi.org/10.1016/j.enggeo.2014.03.003

Xie M, Huang J, Wang L et al (2016) Early landslide detection based on D-InSAR technique at the Wudongde hydropower reservoir. Environ Earth Sci 75:717. https://doi.org/10.1007/s12665-016-5446-3

Xu Q, Li W, Ju Y et al (2020) Multitemporal UAV-based photogrammetry for landslide detection and monitoring in a large area: a case study in the Heifangtai terrace in the Loess Plateau of China. J Mt Sci 17:1826–1839. https://doi.org/10.1007/s11629-020-6064-9

Yi X, Feng W, Meng R et al (2021) Centrifugal model test of deformation law under different reservoir water fluctuation rates: Muyubao landslide case study. IOP Conf Ser: Earth Environ Sci 861:062001. https://doi.org/10.1088/1755-1315/861/6/062001

Yi X, Feng W, Wu Z et al (2020) Toppling deformation characteristics and mechanism of bank slope in Xiluodu Hydropower Station, China. IOP Conf Ser: Earth Environ Sci 570:062007. https://doi.org/10.1088/1755-1315/570/6/062007

Yin Y, Huang B, Chen X et al (2015) Numerical analysis on wave generated by the Qianjiangping landslide in Three Gorges Reservoir, China. Landslides 12:355–364. https://doi.org/10.1007/s10346-015-0564-7

Zhao C, Kang Y, Zhang Q et al (2018) Landslide Identification and Monitoring along the Jinsha River Catchment (Wudongde Reservoir Area), China, Using the InSAR Method. Remote Sens 10:993. https://doi.org/10.3390/rs10070993

Zou Z, Tang H, Criss RE et al (2021) A model for interpreting the deformation mechanism of reservoir landslides in the Three Gorges Reservoir area, China. Nat Hazards Earth Syst Sci 21:517–532. https://doi.org/10.5194/nhess-21-517-2021

Xiaoyu Yi · Wenkai Feng (✉) · Jiawei Dun
State Key Laboratory of Geohazard Prevention and Geoenvironment Protection, Chengdu University of Technology, Chengdu 610059, China

Xiaoyu Yi
Email: xiaou@stu.cdut.edu.cn

Wenkai Feng
Email: fengwenkai@cdut.cn

Xiaoyu Yi · Wenkai Feng · Jiawei Dun
College of Environment and Civil Engineering, Chengdu University of Technology, Chengdu 610059, China

Xiaoyu Yi · Wenkai Feng
Key Laboratory of Geohazard Prevention of Hilly Mountains, Ministry of Natural Resources, Fuzhou 350002, China

Mingtang Wu · Zhiping Ye · Yunfeng Fang · Ping Wang
Zhejiang Huadong Construction Engineering Co., Ltd, Hangzhou 310013, China

Renjiang Li
Relocation & Resettlement Office, China Three Gorges Corporation, Chengdu 610017, China